Light-Induced Passivation in Triple Cation Mixed Halide Perovskites: Interplay between Transport Properties and Surface Chemistry

Stefania Cacovich, Davina Messou, Adrien Bercegol, Solène Béchu, Armelle Yaiche, Hamza Shafique, Jean Rousset, Philip Schulz, Muriel Bouttemy, L. Lombez

ACS APPLIED MATERIALS & INTERFACES

www.acsami.org Research Article

Light-Induced Passivation in Triple Cation Mixed Halide Perovskites: Interplay between Transport Properties and Surface Chemistry

Stefania Cacovich,* Davina Messou, Adrien Bercegol, Solène Béchu, Armelle Yaiche, Hamza Shafique, Jean Rousset, Philip Schulz, Muriel Bouttemy, and Laurent Lombez

Cite This: https://dx.doi.org/10.1021/acsami.0c06844 Read Online

ACCESS | Metrics & More | Article Recommendations | Supporting Information

ABSTRACT: Mixed halide perovskites have attracted a strong interest in the photovoltaic community as a result of their high power conversion efficiency and the solid opportunity to realize low-cost and industry-scalable technology. Light soaking represents one of the most promising approaches to reduce non-radiative recombination processes and thus to optimize device performances. Here, we investigate the effects of 1 sun illumination on state-of-the-art triple cation halide perovskite thin films $Cs_{0.05}(MA_{0.14}, FA_{0.86})_{0.95}$ Pb $(I_{0.84}, Br_{0.16})_3$ by a combined optical and chemical characterization. Competitive passivation and degradation effects on perovskite transport properties have been analyzed by spectrally and time-resolved quantitative imaging luminescence analysis and by X-ray photoemission spectroscopy (XPS). We notice a clear improvement of the optoelectronic properties of the material, with a increase of the quasi fermi level splitting and a corresponding decrease of methylammonium MA^+ for short (up to 1 h) light soaking time. However, after 5 h of light soaking, phase segregation and in-depth oxygen penetration lead to a decrease of the charge mobility.

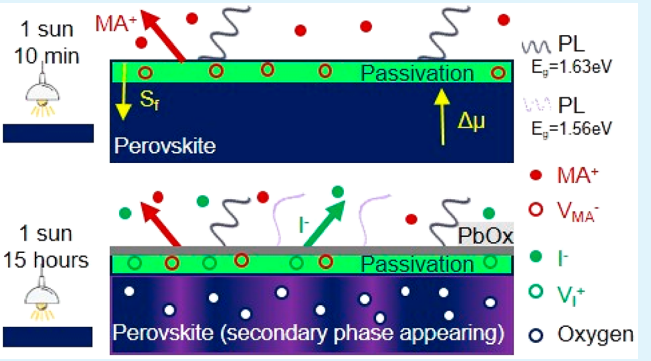

KEYWORDS: *halide perovskites, luminescence imaging, X-ray photoemission spectroscopy, passivation, degradation*

INTRODUCTION

Over the last years, we have witnessed the rise of tremendous interest in research on halide perovskites, particularly for their use in an emergent solar cell technology.[1,2] State-of-the-art perovskite materials exhibit a complex structure and composition including multiple cations and halide alloying. Triple cation halide perovskites proved to be more stable than the archetypal methylammonium lead iodide (MAPI) and lead to higher power conversion efficiency (PCE)[3,4] in corresponding cells. However, the physical and chemical phenomena occurring in different regions in the film (electrode interface, air interface, grain boundaries) and time scales under different stresses (light, oxygen, moisture, temperature, potential) are still not fully understood. Especially, the chemistry at the interfaces has been identified as critically affecting the fundamental optoelectronic properties of the perovskite-based absorber as well as of the working principles of the corresponding solar cells.[5−7] Several surface passivation approaches in full devices have been proposed including the use of 2D perovskite[8] or of organic material such as polymethyl methacrylate (PMMA).[9] These passivation approaches rely on the use of a protective layer preventing in-depth diffusion of reacting agents on chemical passivation or on field-effect passivation.[10]

A long list of degradation processes exists.[11−13] Historically, reversible light-induced transformations on methylammonium lead halide perovskites were first proven by Hoke et al.[14] through steady-state photoluminescence (PL) studies. They observed a red shift of the PL spectrum upon light soaking, which they attributed to halide demixing. The role of light-induced passivation is still under intense debate.[8] Seeming conflicting studies point to both, beneficial or detrimental effects of light soaking on the optoelectronic properties of the materials, strongly dependent on the material chemical composition and the environmental conditions.[15−19] Inhomogeneous optoelectronic properties over the thickness of perovskite thin films after light soaking have been reported and the formation of a band gap gradient have been proven by Barker et al.[20] Additionally, recent studies further reported about in-depth inhomogeneities by evidencing the formation of a highly emissive surface layer upon light soaking in air.[21]

Received: April 14, 2020
Accepted: July 7, 2020
Published: July 7, 2020

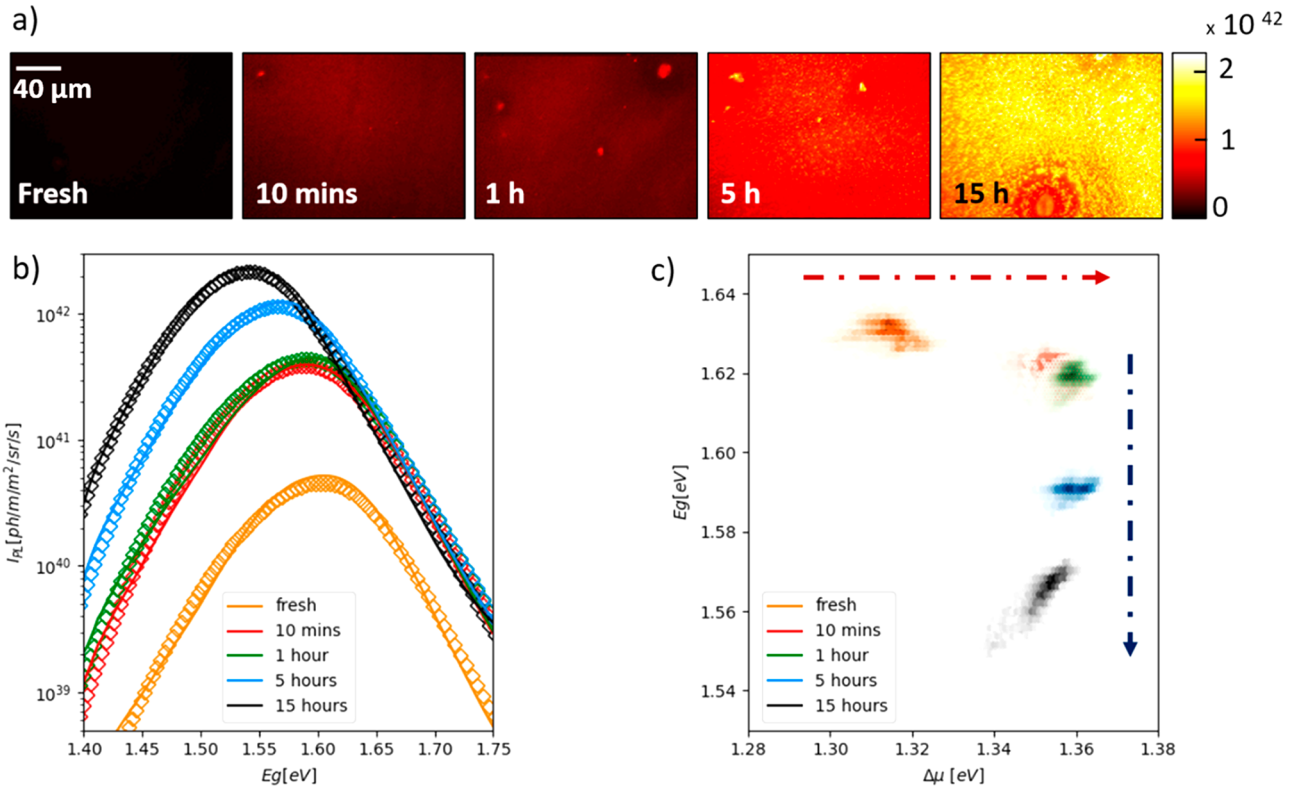

Figure 1. (a) Evolution of the absolute PL signal for different aging times (a different sample for each aging time). (b) Averaged experimental PL spectra and corresponding fitting. (c) Correlation between QFLS and E_g.

Table 1. Main Parameters Calculated with PL Fitting

sample	$\Delta\mu$ (eV)	E_g (eV)	E_u (eV)	$E_g-\Delta\mu$ (meV)
fresh	1.31 [±0.01]	1.63 [±0.01]	0.042 [±0.001]	320
10 min	1.36 [±0.01]	1.62 [±0.01]	0.042 [±0.001]	260
1 h	1.36 [±0.01]	1.62 [±0.01]	0.041 [±0.003]	260
5 h	1.36 [±0.01]	1.59 [±0.01]	0.040 [±0.002]	230
15 h	1.35 [±0.01]	1.56 [±0.01]	0.038 [±0.003]	210

The analysis of changes to the chemical composition of the perovskite surface upon illumination of the sample has been pursued in dedicated studies by X-ray photoemission spectroscopy (XPS). Substantial modifications of the chemical environments[22,23] such as metallic lead (Pb^0) formation[24,25] or change in halide ratio due to ion migration and surface reorganization[19] have been shown. However, only a few publications focus on the detailed effects of light soaking on the perovskite compositions, which currently yield the highest solar cell efficiency, i.e., triple cations lead mixed halide perovskites.[21,26] For this material, Tsai et al.[26] reported the absence of change in the I/Pb ratio for light soaking in an intermediate vacuum. However, our understanding of the link between a change in the perovskite surface composition and the optical properties is limited by the lack of joint investigations that combine surface compositional analysis and advanced optical characterization techniques.

In this present study, we investigated the degradation behavior of triple cation mixed halide perovskites upon light soaking in ambient atmosphere by a combined optical and chemical analysis approach. The chosen sample architecture for this characterization consists of a half-cell taken from an n-i-p perovskite solar cell structure and is composed of the following layer stack: FTO (fluorine doped tin oxide)/compact TiO_2/mesoporous TiO_2/$(Cs_{0.05}(MA_{0.14}, FA_{0.86})_{0.95}$ Pb $(I_{0.84}, Br_{0.16})_3)$. We applied light soaking under realistic operating conditions (T = 25 °C, AM = 1.5G spectrum, 1 sun illumination) and in air (relative humidity ~60%) for a series of samples with exposure times of 10 min, 1 h, 5 h, and 15 h, respectively. We employed multidimensional absolute PL for the determination of the optoelectronic properties of the perovskite films. Using hyperspectral imaging[27] and time-resolved fluorescence imaging (TR-FLIM)[28] we went beyond the classically employed qualitative PL data interpretation and investigated intrinsic material and carrier transport properties with quantitative indicators such as quasi fermi level splitting (QFLS), carrier mobility, and recombination rates. The precise knowledge of such parameters is crucial to understanding light-induced effects under realistic excitation conditions. We pursued the complementary chemical characterization of the sample by XPS on the same batch of samples to determine the evolution of the surface chemical composition with the preceding light soaking time. In addition, we used XPS depth-profiling to assess the changes of the layer stoichiometry that range deeper into the perovskite layer and finally correlated the observed alteration of the optoelectronic properties to the compositional changes. For the studied perovskite films, potentially minute modifications of the cation distribution in the perovskite surface layer, after short light soaking times, can lead to a significant increase in QFLS, whereas prolonged exposure of the film to light eventually results in decomposition and the formation of lead oxide.

https://dx.doi.org/10.1021/acsami.0c06844
ACS Appl. Mater. Interfaces XXXX, XXX, XXX−XXX

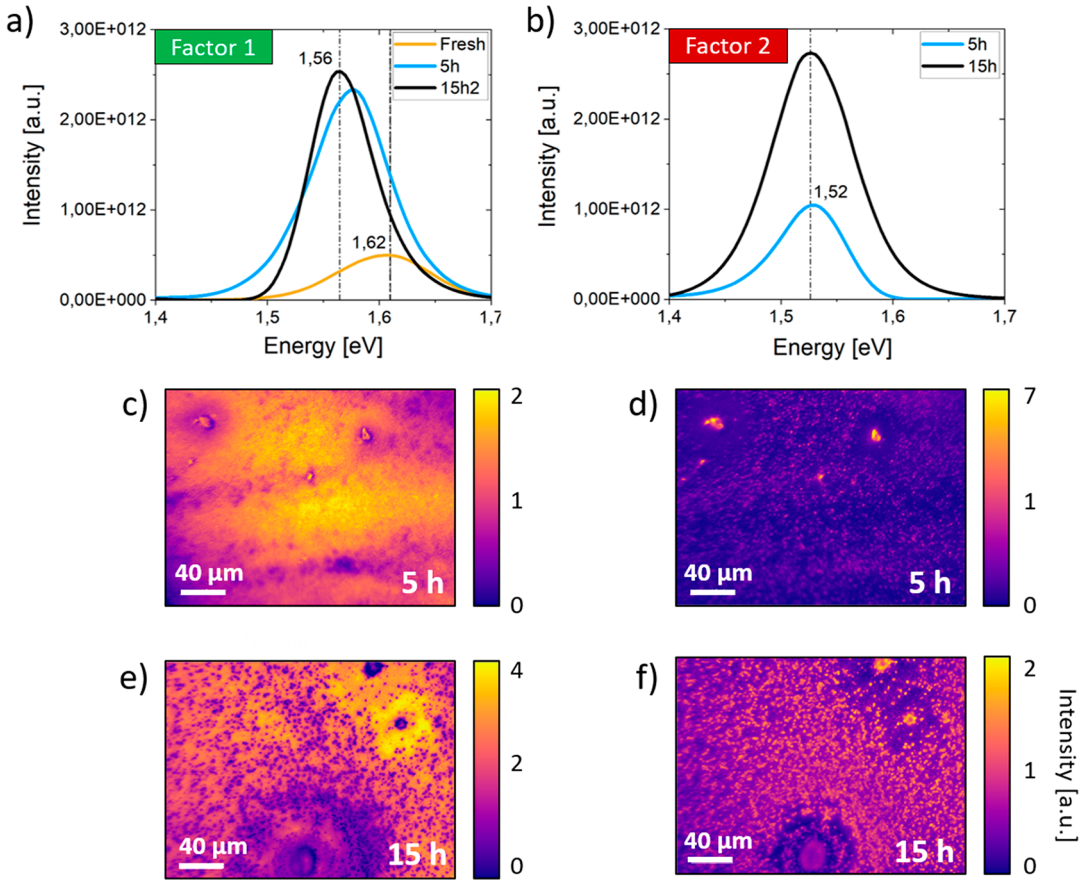

Figure 2. NMF decomposition components. (a) NMF decomposition factor 1 for fresh (peak at 1.62 eV), 5 (peak at 1.59 eV), and 15 h (peak at 1.56 eV). (b) NMF decomposition factor 2 for 5 and 15 h aging times (peak at 1.52 eV). (c) Loading (spatial distribution) of factor 1 for 5 h. (d) Loading (spatial distribution) of factor 2 for 5 h. (e) Loading (spatial distribution) of factor 1 for 15 h. (f) Loading (spatial distribution) of factor 2 for 15 h.

RESULTS AND DISCUSSION

A series of triple cation mixed halide perovskite thin films were light soaked for different times in air. All the samples were kept in dark for 10 min after each light exposure time before being characterized. It is also worth mentioning that the laser light might induce further light soaking effects during PL spectra acquisition, which are however limited to approximately 30 s and are hence not further considered.

In order to limit the laser exposure time, we performed the experiments at 5 (see Figure S1 and Table S2) and 50 suns. Indeed, spectra acquisition at lower excitation fluxes would have required much longer acquisition times to obtain a good signal-to-noise ratio in the photoluminescence spectrum images, which is not easily reconciled with our intention to study light soaking.

We first performed steady-state PL measurements, by acquiring spatially resolved PL spectra (hyperspectral) after different light soaking durations, as reported in Figure 1a. This gives us access to a collection of PL spectra (one per pixel), which can equally be seen as series of spectral images of the sample (one image per wavelength).[29] A first qualitative analysis indicates that increasing the light soaking time results in a constant increase of PL intensity (I_{PL}). Moreover, our setup gives access to I_{PL} intensity in absolute units (luminance units), which allows us to fit the PL spectra by using the approach proposed by Katahara and Hillhouse[30,31] based on the generalized Planck radiation law combined with sub-band gap absorption properties. For this purpose, we adjusted parameters ($\Delta\mu$, T, a(E)) of the following equation to reproduce each spectrum:

$$I_{PL}(E) = \frac{2\pi E^2 a(E)}{h^3 c^2 \exp\left(\frac{E-\Delta\mu}{kT}\right) - 1}$$

where h is the Planck's constant, c as the speed of light, E as the photon energy, a(E) as the absorptivity of the sample taking into account sub-band gap absorption,[30] $\Delta\mu$ as the QFLS, and kT as the thermal energy of the charge carriers. A similar approach to characterize perovskite thin film passivation has been recently reported by Braly et al.[32] in a study aimed at investigating MAPI passivation after *n*-trioctylphosphine oxide (TOPO) treatment.

Representative results of the fitting procedure of the PL spectrum for each sample are shown in Figure 1b. Importantly, we quantified the changes of $\Delta\mu$, the energy gap (E_g), and the sub-band gap absorption (E_u) as shown in Table 1. We first observed a rapid and significant increase of $\Delta\mu$, from 1.31 to 1.36 eV, after 10 min of light soaking already, which indicates that, even after a relatively short amount of time, a passivation effect occurs as a result of a combined exposure of the sample to air and light. Then, with increased aging time, $\Delta\mu$ remained almost constant. Furthermore, after 5 h, we observed a band gap decrease from 1.62 to 1.59 eV, which has previously been linked to perovskite degradation and phase segregation.[21] The driving force of these processes lies in the thermodynamic

https://dx.doi.org/10.1021/acsami.0c06844
ACS Appl. Mater. Interfaces XXXX, XXX, XXX−XXX

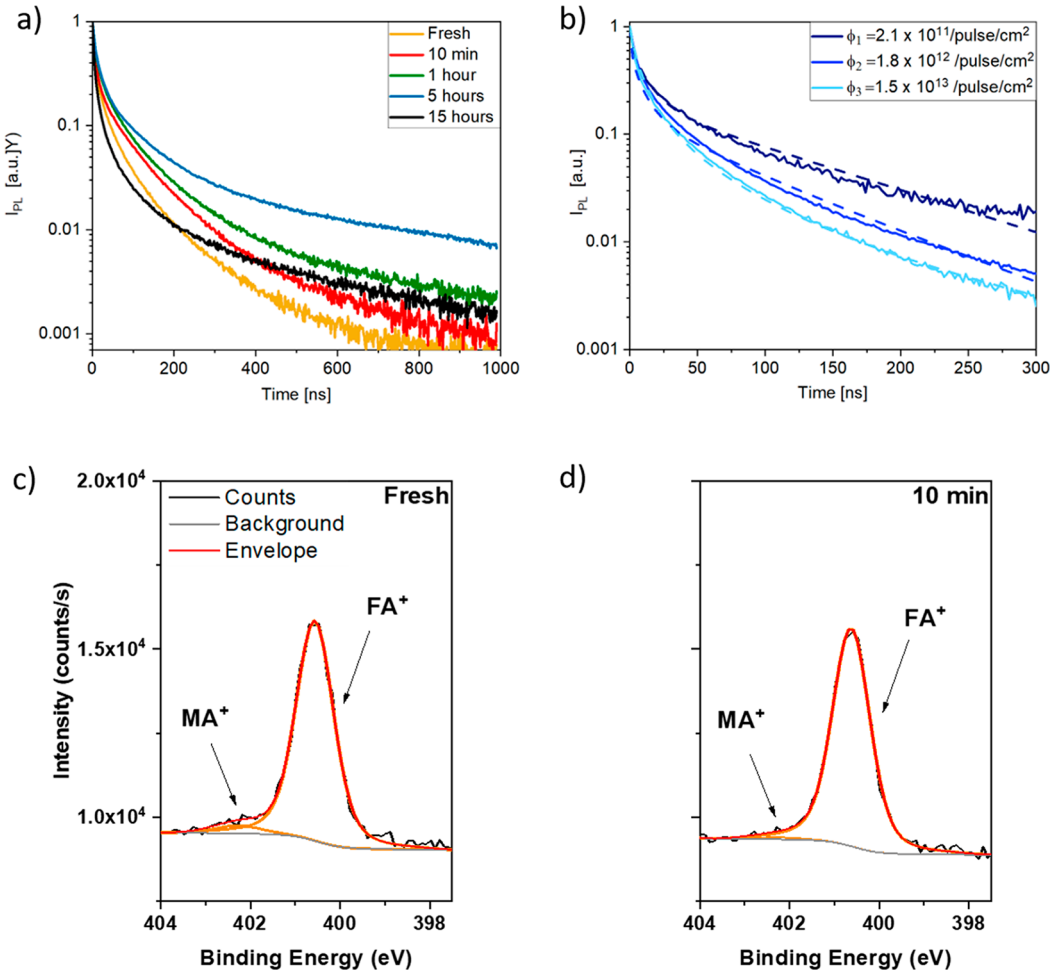

Figure 3. (a) TR-PL transient for different light soaking times. (b) Experimental (solid) and fitted (dashed) curves for the fresh sample at three different values of incident photon flux. (c) Decomposition of the N 1s spectral region for fresh and (d) aged 10 min samples.

photoinstability of perovskite mixed halide systems.[18] Moreover, we report the difference between E_g and $\Delta\mu$ in Table 1, as by comparing materials with different band gaps, this quantity is the indicator for losses quantification. We then plotted the band gap variation as a function of the QFLS for every measured location (pixel) of each sample in Figure 1c. The defect formation can finally be analyzed as the absorption was described by an ideal band-to-band absorption term convoluted with sub-band gap absorption. The tail states decay in the gap with an exponential factor θ = 1.5 and a characteristic energy E_u. For a monoexponential decay of the tail states in the gap, we would have θ = 1 and a E_u that would correspond to the Urbach energy. Further details on the sub-band gap absorption model are reported in the Supporting Information (SI). From this analysis, we note that there is a decrease of the defect concentration, with E_u varying from 0.042 to 0.038 eV, which goes along with the decrease of E_g and $\Delta\mu$ values. It is also of note that this analysis does not reveal yet whether the trap states originate from defects in the bulk or at the interfaces of the perovskite film. The topic will be further discussed along the results of the time-resolved PL (TR-PL) measurements and modeling of recombination.

In order to better assess the phase segregation process in the perovskite film, we applied multivariate analysis to the PL spectral images acquired for different light soaking times. In particular we processed the images by the non-negative factorization (NMF) algorithm from the toolbox *Hyperspy*.[33] The NMF algorithm is a computational method aimed at approximating high-dimensional data by using only a limited number of components. Each spectrum image can be decomposed into a linear combination of factors (Figure 2a,b) with corresponding weights called loadings (Figure 2c–f). NMF decomposition was then applied on the fresh and 5 and 15 h aged samples, resulting in the identification of just one factor in the case of the pristine sample (Figure S2) and two factors in the cases at 5 and 15 h of aging time (factor 1 for high energy and factor 2 for low-energy contribution). Although the two factors do not have *a priori* a strict physical meaning, they can provide insight on the perovskite evolution. We attribute the first factor to the characteristic PL peak of the halide perovskite thin films (as it is the only one represented before light soaking), which increases in intensity with time. The peak is shifted from 1.62 eV in the fresh sample to 1.56 eV in the aged ones (Figure 2a). Moreover, a second factor at 1.52 eV started to appear after 5 h of light soaking, which happens to correspond to the time when the band gap of the material starts evolving (Figure 2b). The corresponding loadings shown in Figure 2 display a clear spatial anticorrelation of the two factors, suggesting the formation of two different emissive species in the perovskite layer, one at a lower energy and the other at a higher energy (more precisely when looking at

https://dx.doi.org/10.1021/acsami.0c06844
ACS Appl. Mater. Interfaces XXXX, XXX, XXX−XXX

Figure 2c vs d for 5 h of light soaking and Figure 2e vs f for 15 h of light soaking).

To further investigate the effect of the passivation process on the transport properties of the materials, we performed time-resolved PL analysis. We observed a clear variation of the decays in the different samples, as reported in Figure 3a. We performed a power dependence study,[34,35] and we fitted the experimental curves with the diffusion equation with interface recombination as boundary conditions (S_{air} is the front interface recombination velocity and S_{back} is the back interface recombination velocity):

$$\frac{\partial n}{\partial t} = -R^*_{eh}n^2 - \frac{n}{\tau_n} + D\frac{\partial n}{\partial z}$$

$$\frac{D\partial n}{\partial z} = S_{air}n$$

$$\frac{D\partial n}{\partial z} = S_{back}n$$

where n is the charge carrier concentration, R^*_{eh} is the external radiative coefficient, τ_n is the Shockley–Read–Hall carrier lifetime, and D is the diffusion coefficient

We took the back interface as a reference ($S_{back} = 0$) since the back interface is assumed to not vary with time contrary to the front one. The samples were illuminated from the top surface (perovskite). The intensity of the incident photon flux was varied over 2 orders of magnitude $\varphi_1 = 2.1 \times 10^{11}$, $\varphi_2 = 1.8 \times 10^{12}$, and $\varphi_3 = 1.5 \times 10^{13}$/pulse/cm^2, as shown in Figure 3b in the case of the pristine sample. The fitting procedure is done simultaneously for the data from all three excitation fluxes to increase the accuracy of the results. We report the fitted values of the diffusion coefficient, radiative recombination rate R^*_{eh}, and surface recombination rate in Table 2.

Table 2. Values for the Diffusion Coefficient D, Radiative Recombination Rate R^*_{eh}, and Surface Recombination Rate S_{air} Obtained from TRPL Data Analysis Using the Diffusion Equation

sample	D [$\times 10^{-3}$ cm^2/s]	R^*_{eh} [$\times 10^{-11}$ cm^3/s]	S_{air} [cm/s]
fresh	1.7 [±0.1]	6.2 [±0.2]	1020 [±80]
10 min	1.3 [±0.1]	4.2 [±0.2]	114 [±15]
1 h	1.2 [±0.1]	5.8 [±0.4]	210 [±10]
5 h	0.7 [±0.1]	3.7 [±0.1]	200 [±7]
15 h	1.0 [±0.1]	16 [±0.1]	340 [±20]

As we increased the light soaking time, we observe a decreased of the surface recombination as well as a reduction of the diffusion coefficient and therefore also of the carrier mobility. We ascribe these observations to an effective passivation of the perovskite film surface, indicated by the immediate decrease of S_{air}, followed by steady materials degradation for longer light soaking times, consistent with a slower, gradual decrease in D. These results match the data obtained for the steady-state PL experiment in the previous section, in which we found an immediate increase in QFLS after several minutes of light soaking, corresponding to reduced surface recombination, along with a gradual decrease of the band gap for longer light soaking times, which is consistent with a slower material's degradation process. Concomitantly to the PL measurements, we investigated by XPS the chemistry of the perovskite layers, which were aged under illumination in air for different light soaking times. Both composition and chemical environments changes at the surface of the film were studied as well as in-depth elements distributions and associated stoichiometric modifications in the bulk film by using complementary Ar^+ depth-profiling. All samples investigated originated from the same batch to allow for a direct comparison between the XPS and PL analysis. In addition, all light-soaked samples were introduced simultaneously in the XPS spectrometer, enabling us to control the transfer step and track with accuracy the chemical modifications along aging. Storage of the samples in the vacuum system (in dark) was not found to further degrade, reconstitute, or change the surface chemistry of the light-soaked films (Table S2 and Figure S4). A sample issued from a similar batch and aged for 6 days at atmosphere in the dark, i.e., without light soaking, was also characterized as an additional point of reference. Note that the spatial resolutions of PL and XPS are not the same. Indeed, with a 400 μm spot size, the XPS information is roughly averaged over the entire PL image area but only probes a few nanometers in depth. The measured distribution of the constitutive chemical elements at the surface as a function of the aging time is captured in Table S1, while we show the spectra of the N 1s photopeak perovskite films aged for short time (10 min) in Figure 3c,d. The MA^+ contribution (402.4 ± 0.2 eV) disappears with light soaking, while the FA^+ contribution (400.9 ± 0.2 eV) decreases at a lower rate (see Table S1). We can thus observe a direct link between the loss of the MA^+ contribution in the perovskite surface layer and the decrease of the front interface recombination velocity, suggesting that the changes in the cation composition play a key role in the passivation processes occurring in triple cation halide perovskite thin films.

XPS high-resolution spectra of the perovskite films aged for 0, 5, and 15 h are shown in Figure 4. Additional spectra of the films aged for 10 min and 1 h can be found in the Supporting Information (Figure S5). XPS sequence durations were optimized to ensure the reliability of the measurements, without inducing noticeable degradation from the X-ray irradiation (Figure S6).[36] By verifying the reproducibility of our approach, no significant difference in the surface chemical composition of the as-prepared reference sample and the reference sample, which was a week-long aged in ambient and in dark, can be discerned (see Figure S4). Particularly, no variation in the magnitude of the oxygen content and chemical state is observed. Thus, in the dark, the surface stoichiometry of the triple cation lead mixed halide perovskite film appears to be stable despite exposure to extrinsic species such as O_2 and H_2O at least over almost 1 week, consistent with previous studies of $MAPbI_3$.[12] Similarly, in one recent study, we observed that the transport properties of a triple cation mixed halide perovskite thin film remain constant after aging in dark in ambient air for 9 days.[37]

In contrast to that, prolonged aging in air under illumination leads to substantial changes of the surface chemistry. We begin with a description of the metal halide sublattice species, where we observed a progressive enrichment of Br and Pb at the surface and a concomitant decrease of the I content. Surfaces observed are enriched in iodine, since the initial I/Pb ratio is close to 3.2 (instead of 2.5 theoretically). This was already reported in the literature[38,39] and can be due to a termination of the surface with MAI. Specifically, the Br/(I+Br) ratio increases from 0.15 ± 0.03 for the as-prepared sample to 0.41 ± 0.03 after 15 h of light soaking in air while the Pb/(I+Br)

https://dx.doi.org/10.1021/acsami.0c06844
ACS Appl. Mater. Interfaces XXXX, XXX, XXX−XXX

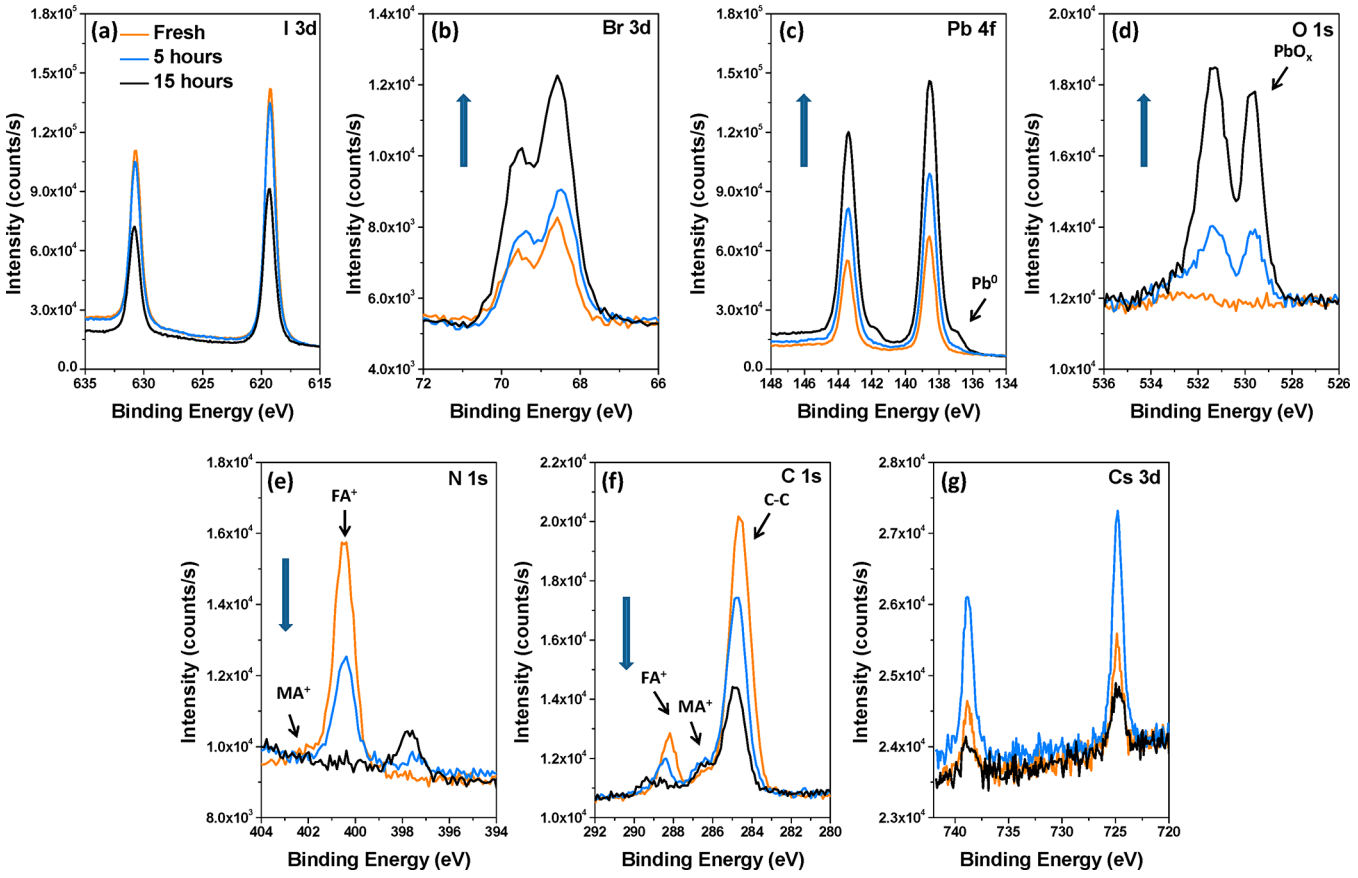

Figure 4. High-energy-resolution XPS spectra comparison of an as prepared triple cation mixed halide perovskite film (orange line) and corresponding layer aged under light soaking in ambient atmosphere for 5 (blue line) and 15 h (black line): (a) I 3d, (b) Br 3d, (c) Pb 4f, (d) O 1s, (e) N 1s, (f) C 1s, and (g) Cs 3d spectral regions.

ratio increases from 0.27 ± 0.03 to 0.86 ± 0.03. Apart from this stoichiometric change, we discerned no further apparent variation in the chemical environment of the halide species, as binding energy position and full-width at half-maximum (fwhm) of the I and Br peaks remain steady, as seen in Figure 4a,b. The case is different for the Pb content (Figure 4c), where two distinct changes can be identified. First, we saw the appearance of an additional Pb $4f_{7/2}$ peak centered at 136.8 ± 0.2 eV, hence corresponding to the Pb^0 species after 15 h of light soaking.[40] The formation of metallic lead has been observed before as a presumed degradation product in halide perovskite samples as a function of exposure to X-ray radiation[41,42] or laser illumination.[40] Second, the initial Pb^{2+} contribution, centered at 138.5 eV binding energy, exhibited an increase of the fwhm from 0.81 ± 0.05 eV for the as-prepared perovskite layer to 1.01 ± 0.05 eV for the film after 15 h of light soaking. This observation is indicative of a change of the lead complexation from the perovskite ABX_3 structure to lead dihalides (PbX_2) and potentially PbO_x.[43,44]

In addition to these marked chemical changes, we observed XPS peak shifts, which suggest a change in the surface electronic properties after light soaking of the samples in air. Even after 10 min of light soaking we observed a uniform shift of 0.5 eV of all core levels with respect to the Fermi level of the spectrometer toward lower binding energies (see Figure S7 to compare the I 3d and Pb 4f core levels plotted with respect to E_F). This shift is consistent with earlier reports of the saturation of undercoordinated Pb^{2+} sites at the sample surface, which act as donor defect states and hence let the sample appear more n-type at the surface.[45] After passivation, i.e., light soaking, this surface band bending is alleviated and the surface appears to be rather intrinsic with the Fermi level in the middle of the gap.

Concerning the potential complexation of PbO_x species, we found a notable increase of the O content concomitant to the decrease of the halide and in particular the iodine content with sample aging, as the O/(I+Br) ratio rises from 0.06 ± 0.03 for the as-prepared sample to 0.80 ± 0.03 for the sample aged for 15 h. The identified oxygen components were found in a range of chemical states. In case of the as-prepared perovskite film, we found only a minor contribution of O on the perovskite surface, which is related to minimal exposure of the film to ambient atmosphere during the transfer from sample preparation to the XPS analysis chamber. The corresponding O 1s peak binding energy is 532.6 ± 0.2 eV, which had been attributed to H_2O in hydrated perovskite surfaces.[19] After aging under illumination in air, two additional contributions appear, in agreement with the previous work of Anaya et al.[19] The contribution located at 531.3 ± 0.2 eV corresponds to O_2^-, i.e., superoxide, which can occupy former iodine vacancies in the ABX_3 lattice, as has been seen for oxygen-induced photodegradation of $MAPbI_3$,[34] while the second contribution centered at 529.6 ± 0.2 eV corresponds to O^{2-} as in metal oxide species such as PbO.[46] The amount of O_2^- and O^{2-} steeply increases with light exposure, and they are thus inherently linked to the degradation process, which confirms the formation of PbO_x.[44] We now turn to the chemical changes to the A-site cations, starting with a discussion of the N 1s

https://dx.doi.org/10.1021/acsami.0c06844
ACS Appl. Mater. Interfaces XXXX, XXX, XXX−XXX

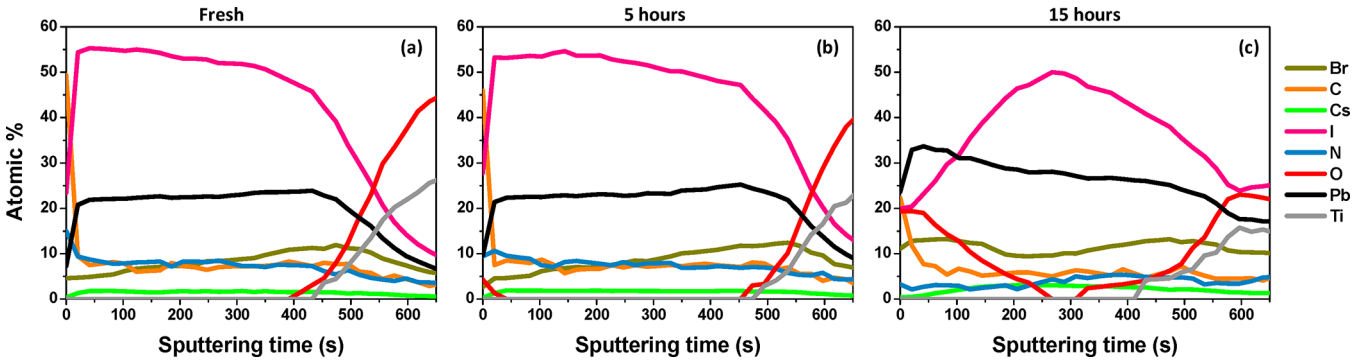

Figure 5. XPS depth profile (Ar^+, 1000 eV) comparison of (a) fresh triple cation perovskite and (b) 5 and (c) 15 h aged perovskite. Quantification has been made for peak fitting in the Br 3d, Cs 3d, I 3d, C 1s, N 1s, Pb 4f, and O 1s regions. Depth profiles for the films with intermediate light soaking times are displayed in the Supporting Information (Figure S8).

photopeak (Figure 4e). As already observed for short light soaking times (10 min), the MA^+ contribution[47] (402.4 ± 0.2 eV) fully disappears with light soaking while the FA^+ contribution[47] (400.9 ± 0.2 eV) decreases at a lower rate. Meanwhile, a new contribution at 398.3 ± 0.2 eV starts to appear after 5 h of light soaking and remains as a last single component after 15 h of light soaking. This contribution at a lower binding energy has already been reported and could be related to NH_3 release under light,[23] due to the C−N chemical bond degradation in the FA^+ and MA^+ components.[48]

The observations are consistent with the evolution of the C 1s peaks (Figure 4f) that shows a decrease of the C 1s signal originating from the imidine bond in FA^+ (288.3 ± 0.2 eV) with aging time. However, a precise quantification of the carbon contributions is limited due to the convolution with the signal from adventitious carbon species. Especially, the discrimination between carbon in MA^+ species at binding energies and C−O species at approximately 286.4 eV binding energy becomes challenging,[31] notably at the appearance of a contribution at 289.2 ± 0.2 eV related to new C−N species as degradation products. Finally, for the Cs cations, we found a progressive increase of the fwhm Cs 3d peak with aging time from 0.92 ± 0.05 eV initially to 1.34 ± 0.05 eV after 15 h of light soaking. A similar observation has been made for fully inorganic $CsPbBr_3$ perovskite films and is consistent with the emergence of Cs_2CO_3 as a degradation product.[49]

In order to track the permeation of the degradation process through the perovskite layer, we performed XPS depth profiling of the as-prepared and the aged perovskite films down to the TiO_2 transport layer (Figure 5 for fresh and 5 and 15 h aged spectra; Figure S8 for 10 min and 1 h aged ones). The layer composition of the as-prepared perovskite film is in good agreement with ToF-SIMS data for comparable perovskites films found in the literature.[50,51] We thus report constant profiles of I, Pb, and Cs throughout the layer and an accumulation of Br over I toward the perovskite/TiO_2 interface. The surface of the perovskite film is enriched in C and N, while oxygen species are only present in the very surface layer of few nanometers in thickness. The profile of the sample aged for 5 h remains similar, with the exception of small changes of the surface composition (see Table S1) and a slightly higher ratio of O incorporation within the subsurface region. However, after 15 h of light soaking, we observed distinct changes to the perovskite film composition. The top layers of the film are strongly enriched in Pb, Br, and O content and show a deficiency in I and Cs. For a sputtering time of 250 s, corresponding to a crater depth of several tens of nanometers, this trend is slowly reversing toward the film bulk with the I and Cs content increasing and the Pb, Br, and O content decreasing, approaching the compositional ratio found for the as-prepared perovskite film. Nonetheless, the films remain deficient in C, N, and I, which is presumably linked to the evaporation of these volatile species while the lead halide and lead oxide degradation products lead to a Pb excess compared to the as-prepared films. These stoichiometric changes track even down to the bulk of the perovskite films.

Notably, the oxygen contribution can be attributed to adventitious species and superoxides for the very surface layer and PbO_x, with the O 1s signal at 529.4 ± 0.2 eV, further down into the bulk film. Both contributions are clearly distinct from O in the TiO_2 substrate layer, which is revealed only after 400 s of sputtering (see the Supporting Information, Figure S9).

As a concluding remark, we note that the depth-profiling process can show marked differences if the structural parameters of the layer are changed. This seems to be the case for the sample aged for 15 h, which exhibits cavity formation as seen in scanning electron microscopy images (Figure S3), which is consistent with the loss of C, N, and I reported above. This leads to a significant perturbation of the stoichiometry analysis at the buried mp-TiO_2/perovskite interface, which seems to appear less sharp. Nonetheless, all qualitative trends of the compositional data for the top part of the perovskite film aged for 15 h, down to the first appearance of the TiO_2 signal (>300−400 s sputtering time), remain unaffected.

The summary results help to explain the previously presented hyperspectral and time-resolved photoluminescence data. Changes in the Br to I ratio across the layer demonstrate halide segregation, which is accordant to the occurrence of two emissive species and an overall decrease in the band gap. While the increased Br to I ratio would generally indicate an increase in band gap and more pronounced split components of emissive species, our joint XPS and PL results indicate that the bromine rich regions, particularly in the top layer of the light-soaked film, are not as emissive. One possible explanation lies in the partial formation of $PbBr_2$, which is in accordance to the concomitant loss of organic cations observed in the decreased nitrogen signal after long light soaking times. Note that the segregation also occurs laterally on the scale of nanometers to several micrometers and is thus laterally averaged in the XPS analysis area. As a final point, the formation of PbO_x as well as

https://dx.doi.org/10.1021/acsami.0c06844
ACS Appl. Mater. Interfaces XXXX, XXX, XXX−XXX

the loss of organic cation and halide species are consistent with the decrease of the carrier diffusion coefficient.

CONCLUSION

We performed a comprehensive study of triple cation mixed halide perovskite photophysics, focusing both on transport properties and surface chemistry. In particular, we proposed that short light time exposure (10 min or 1 h) results in an enhancement of the optoelectronic properties of the material, as evidenced by the increase of the QFLS of the perovskite thin films from 1.31 to 1.36 eV. In the same time scale, the sole noticeable evolution of the surface chemistry is related to the N environment, with a small decrease of the MA^+ content from the as deposited sample surface to 10 min of light soaking, while it disappears for longer times. For longer light soaking times (5 and 15 h), the formation of persistent chemical species is observed on the samples. The aforementioned $(E_g - \Delta\mu)$ values show a drastic drop in non-radiative recombination, and the time-resolved PL measurements confirmed that the passivated recombination centers are located at the front interface (perovskite/air). As such, both steady-state and transient measurements evidence a surface passivation effect. The modifications of the chemical environments suggest the formation of a stable PbO_x layer starting from 5 h of continuous light soaking in an air atmosphere. The benign formation of this oxidized layer goes along with sample degradation. Starting from 5 h of light soaking, a phase segregation appears, leading to iodine-rich-emitting regions and to a degradation of the transport properties of the material. This is evidenced by time-resolved measurements showing a constant decrease of the diffusion coefficient D and therefore of the charge mobility (Figure 3). XPS depth profiles indicate that the main responsibility of this sample degradation is the oxygen diffusion through the perovskite active layer. Additionally, there is a halide redistribution with an iodine depletion layer at the top interface and a bromine homogenization. This is apparently in contrast with PL measurements where a red shift was observed (from 1.63 to 1.56 eV), thus indicating the presence of iodine-rich-emitting regions. A possible explanation is that bromine-rich species do not contribute to the PL emission, which would happen as the charge carrier first migrates to lower band gap iodine-rich regions and then recombines radiatively. To conclude, this work provides new insight in the competing reaction occurring in triple cation mixed halide perovskite. The use of advanced and complementary characterization techniques allowed us to deeply investigate the phenomena leading to surface passivation and to sample degradation. The fine control of the benign species at the top interface of the perovskite might lead to an increase of device performances opening up new solutions for improving and stabilizing perovskite-based devices. However, further studies aimed at investigating the reversibility of the observed phenomena and their influence on the photovoltaic parameters are required to fully exploit the potential of such passivation approach.

EXPERIMENTAL SECTION

Sample Preparation. Fluorine-doped tin oxide (FTO) covered glass substrates (Solems) were cleaned by etching with Zn powder and HCl (4 M). The substrates were sonicated for 1 h in an RBS detergent solution (2 vol %), rinsed with deionized water and ethanol, ultrasonicated in ethanol, dried, and annealed to 500 °C. Subsequently, a TiO_2 hole blocking layer was prepared by spray pyrolysis deposition at 450 °C from a precursor solution made of 0.6 mL of titanium diisopropoxide bis(acetylacetonate) (75% in 2-propanol, Sigma-Aldrich) and 0.4 mL of acetylacetone (Sigma-Aldrich) in 9 mL of ethanol as a solvent and O_2 as a carrier gas. The mesoporous TiO_2 (mp-TiO_2) layer was prepared by spin-coating a solution of TiO_2 paste (30NR-D from Dyesol) in ethanol (1:7 weight ratio) at 4000 rpm for 30 s. The films were then sintered in a sequential heating process (5 min at 125 °C, 5 min at 325 °C, 5 min at 375 °C, 15 min at 450 °C, and 30 min at 500 °C). The substrates were finally transferred into a nitrogen-filled glovebox for the perovskite film deposition. A double cation perovskite solution, $(MA_{0.17}FA_{0.83})Pb(Br_{0.17}I_{0.83})_3$ was prepared by dissolving 1.10 M PbI_2 (TCI Chemicals), 0.20 M $PbBr_2$ (Alfa Aesar), 1.00 M formamidinium iodide (FAI, Dyesol), and 0.20 M methylammonium bromide (MABr, Dyesol) in a mixture of DMSO/DMF (4:1 in v/v) as solvent. In order to obtain the triple cations perovskite, i.e., $Cs_x(MA_{0.17}FA_{0.83})_{1-x}Pb(Br_{0.17}I_{0.83})_3$, the required quantity of Cs^+ was additionally injected from a precursor solution of CsI (Sigma-Aldrich) 1.50 M in DMSO solvent. The solution, after 2 h of stirring in a magnetic mixer, was spin-coated onto the mesoporous TiO_2 layers by following a double plateau. First, 35 μL of the perovskite solution was spin-coated at the rotation of 2000 rpm for 10 s at an acceleration of 1000 rpm/sec. Then, 100 μL of chlorobenzene was spin-coated at a speed of 6000 rpm for 30 s. After deposition, the perovskite films were submitted to an annealing treatment at the temperature of 100 °C for 30 min in a nitrogen glovebox. The thickness of the perovskite thin films was approximately 400 nm.

Time-Resolved Luminescence. Wide-field illumination imaging was realized with a TR-FLIM setup. The system is composed of a pulsed laser Talisker (θ = 532 nm, f = 200 kHz), an intensified electron-multiplied camera CCD (em-ICCD, PIMAX4, Princeton Instruments), and a home-built opto-mechanical excitation-collection setup. The camera gating time was varied with a 2 ns step from 0 to 1 μs. The photoluminescence was collected through a Nikon 50× objective. The PL was filtered through short-pass and long-pass filters (DMLP650R and FES750, Thorlabs). Acquisitions were post-treated using Matlab.

Hyperspectral Luminescence Imaging. The hyperspectral imaging system records a luminescence intensity signal along three dimensions $\{x,y,\lambda\}$. Its main components are a home-built microscope with Thorlabs optomechanical elements, a 2D bandpass filtering system from company PhotonEtc with 2 nm resolution, and finally a 1Mpix silicon-based CCD camera PCO1300. The sample is illuminated (λ = 532 nm) through an infinity-corrected ×50 Nikon objective with numerical aperture of 0.8, and the luminescence is collected through the same objective. The excitation beam and luminescence signals are separated with appropriate dichroic beam splitter and filters. The 2D luminescence signal is corrected for each pixel of the sensor from the spectral transmissions along all the optical path, from the read noise and dark current noise of the camera, and from the spatial inhomogeneity of the optical system (flat-field). The spatial resolution is 1 μm. Post-treatment of the data cubes includes a deconvolution and fit to the generalized Planck law, which are realized with a dedicated Matlab routine employing the Levenberg–Marquardt algorithm.

X-ray Photoelectron Spectroscopy (XPS). Samples were transferred after light soaking under a low vacuum (secondary vacuum range) in dark conditions using a transfer vessel to ensure no supplementary modifications on surfaces, particularly sensitivity to humidity and light. The transfer to the XPS analysis chamber was minimized to 2 h. XPS surface chemical analyses were carried out with a Thermo Electron K-Alpha+ spectrometer using a monochromatic Al Kα X-ray source (1486.6 eV). The Thermo Electron K-Alpha spectrometer procedure was used to calibrate the spectrometer and verified using Cu and Au samples following the ASTM-E-902–94 standard procedure.

The X-ray spot size was 400 μm. High-energy-resolution spectra were acquired using a constant analyzer energy (CAE) mode of 20 and 0.1 eV as the energy step size, without charge compensation. The energy scale was calibrated with respect to the C 1s peak settled at

https://dx.doi.org/10.1021/acsami.0c06844
ACS Appl. Mater. Interfaces XXXX, XXX, XXX–XXX

284.6 eV to facilitate comparison of chemical shifts between the various samples investigated.

Sputtering was performed with Ar^+ monatomic ions at an energy level of 1000 eV and 10 mA current density for 800 s. Data were processed using the Thermo Fisher Scientific Avantage© data system. The acquisition sequence was optimized to limit the X-ray irradiation exposure (1 h), and the stability of the perovskite layer was controlled by recording two survey spectra: one at the start of the acquisition sequence and one at the end (CAE of 100 and 1.0 eV energy step size). Three sets of samples were measured to obtain statistic data and guarantee the reliability of the information obtained.

■ ASSOCIATED CONTENT

Supporting Information

The Supporting Information is available free of charge at https://pubs.acs.org/doi/10.1021/acsami.0c06844.

Discussions of I_{PL} spectra and NMF analysis, figures of PL spectra, loading and factor from NMF on the fresh sample PL spectrum image, SEM images, XPS spectra, XPS depth profiles, and evolution of the O 1s, Pb 4f, and N 1s photopeaks, and tables of main optoelectronic parameters and XPS atomic percentages (PDF)

■ AUTHOR INFORMATION

Corresponding Author

Stefania Cacovich − *IPVF, Institut Photovoltaïque d'Ile-de-France, 91120 Palaiseau, France; École Polytechnique, IPVF, UMR 9006, CNRS, 91120 Palaiseau, France;* orcid.org/0000-0002-6402-4816; Email: stefania.cacovich@cnrs.fr

Authors

Davina Messou − *IPVF, Institut Photovoltaïque d'Ile-de-France, 91120 Palaiseau, France; Université Paris-Saclay, UVSQ, CNRS, UMR 8180, Institut Lavoisier de Versailles, 78000 Versailles, France*

Adrien Bercegol − *IPVF, Institut Photovoltaïque d'Ile-de-France, 91120 Palaiseau, France; EDF R&D, 91120 Palaiseau, France;* orcid.org/0000-0003-3531-5312

Solène Béchu − *IPVF, Institut Photovoltaïque d'Ile-de-France, 91120 Palaiseau, France; Université Paris-Saclay, UVSQ, CNRS, UMR 8180, Institut Lavoisier de Versailles, 78000 Versailles, France*

Armelle Yaiche − *IPVF, Institut Photovoltaïque d'Ile-de-France, 91120 Palaiseau, France; EDF R&D, 91120 Palaiseau, France*

Hamza Shafique − *École Polytechnique, IPVF, UMR 9006, CNRS, 91120 Palaiseau, France*

Jean Rousset − *IPVF, Institut Photovoltaïque d'Ile-de-France, 91120 Palaiseau, France; EDF R&D, 91120 Palaiseau, France*

Philip Schulz − *IPVF, Institut Photovoltaïque d'Ile-de-France, 91120 Palaiseau, France; École Polytechnique, IPVF, UMR 9006, CNRS, 91120 Palaiseau, France;* orcid.org/0000-0002-8177-0108

Muriel Bouttemy − *IPVF, Institut Photovoltaïque d'Ile-de-France, 91120 Palaiseau, France; Université Paris-Saclay, UVSQ, CNRS, UMR 8180, Institut Lavoisier de Versailles, 78000 Versailles, France*

Laurent Lombez − *IPVF, Institut Photovoltaïque d'Ile-de-France, 91120 Palaiseau, France; École Polytechnique, IPVF, UMR 9006, CNRS, 91120 Palaiseau, France;* orcid.org/0000-0001-7895-913X

Complete contact information is available at: https://pubs.acs.org/10.1021/acsami.0c06844

Notes

The authors declare no competing financial interest.

■ ACKNOWLEDGMENTS

This project has been supported by the French Government in the frame of the program of investment for the future (Program d'Investissement d'Avenir - ANRIEED-002-01). S.C. would like to thank funding from the European Union's Horizon 2020 research and innovation programme under the Marie Skłodowoska-Curie Grant Agreement N 845612. P.S. would like to acknowledge the French Agence Nationale de la Recherche for funding under contract no. ANR-17-MPGA-0012.

■ REFERENCES

(1) Kim, H.-S.; Hagfeldt, A.; Park, N.-G. Morphological and Compositional Progress in Halide Perovskite Solar Cells. *Chem. Commun.* **2019**, *55* (9), 1192−1200.

(2) Stranks, S. D.; Snaith, H. J. Metal-Halide Perovskites for Photovoltaic and Light-Emitting Devices. *Nat. Nanotechnol.* **2015**, *10* (5), 391−402.

(3) Saliba, M.; Matsui, T.; Seo, J.-Y.; Domanski, K.; Correa-Baena, J.-P.; Nazeeruddin, M. K.; Zakeeruddin, S. M.; Tress, W.; Abate, A.; Hagfeldt, A.; Grätzel, M. Cesium-Containing Triple Cation Perovskite Solar Cells: Improved Stability, Reproducibility and High Efficiency. *Energy Environ. Sci.* **2016**, *9* (6), 1989−1997.

(4) Ono, L. K.; Juarez-Perez, E. J.; Qi, Y. Progress on Perovskite Materials and Solar Cells with Mixed Cations and Halide Anions. *ACS Appl. Mater. Interfaces* **2017**, *9* (36), 30197−30246.

(5) Schulz, P.; Cahen, D.; Kahn, A. Halide Perovskites: Is It All about the Interfaces? *Chem. Rev.* **2019**, *119* (5), 3349−3417.

(6) Ono, L. K.; Qi, Y. Surface and Interface Aspects of Organometal Halide Perovskite Materials and Solar Cells. *J. Phys. Chem. Lett.* **2016**, *7* (22), 4764−4794.

(7) Shallcross, R. C.; Zheng, Y.; Saavedra, S. S.; Armstrong, N. R. Determining Band-Edge Energies and Morphology-Dependent Stability of Formamidinium Lead Perovskite Films Using Spectroelectrochemistry and Photoelectron Spectroscopy. *J. Am. Chem. Soc.* **2017**, *139* (13), 4866−4878.

(8) Liu, Y.; Akin, S.; Pan, L.; Uchida, R.; Arora, N.; Milić, J. V.; Hinderhofer, A.; Schreiber, F.; Uhl, A. R.; Zakeeruddin, S. M.; Hagfeldt, A.; Dar, M. I.; Grätzel, M. Ultrahydrophobic 3D/2D Fluoroarene Bilayer-Based Water-Resistant Perovskite Solar Cells with Efficiencies Exceeding 22%. *Science Advances* **2019**, *5* (6), No. eaaw2543.

(9) Peng, J.; Wu, Y.; Ye, W.; Jacobs, D. A.; Shen, H.; Fu, X.; Wan, Y.; Duong, T.; Wu, N.; Barugkin, C.; Nguyen, H. T.; Zhong, D.; Li, J.; Lu, T.; Liu, Y.; Lockrey, M. N.; Weber, K. J.; Catchpole, K. R.; White, T. P. Interface Passivation Using Ultrathin Polymer−Fullerene Films for High-Efficiency Perovskite Solar Cells with Negligible Hysteresis. *Energy Environ. Sci.* **2017**, *10* (8), 1792−1800.

(10) Chen, B.; Rudd, P. N.; Yang, S.; Yuan, Y.; Huang, J. Imperfections and Their Passivation in Halide Perovskite Solar Cells. *Chem. Soc. Rev.* **2019**, *48* (14), 3842−3867.

(11) Berhe, T. A.; Su, W.-N.; Chen, C.-H.; Pan, C.-J.; Cheng, J.-H.; Chen, H.-M.; Tsai, M.-C.; Chen, L.-Y.; Dubale, A. A.; Hwang, B.-J. Organometal Halide Perovskite Solar Cells: Degradation and Stability. *Energy Environ. Sci.* **2016**, *9* (2), 323−356.

(12) Boyd, C. C.; Cheacharoen, R.; Leijtens, T.; McGehee, M. D. Understanding Degradation Mechanisms and Improving Stability of Perovskite Photovoltaics. *Chem. Rev.* **2019**, *119* (5), 3418−3451.

(13) Cacovich, S.; Divitini, G.; Ireland, C.; Matteocci, F.; Di Carlo, A.; Ducati, C. Elemental Mapping of Perovskite Solar Cells by Using Multivariate Analysis: An Insight into Degradation Processes. *ChemSusChem* **2016**, *9* (18), 2673−2678.

(14) Hoke, E. T.; Slotcavage, D. J.; Dohner, E. R.; Bowring, A. R.; Karunadasa, H. I.; McGehee, M. D. Reversible Photo-Induced Trap

Formation in Mixed-Halide Hybrid Perovskites for Photovoltaics. *Chemical Science* **2015**, *6* (1), 613−617.
(15) Motti, S. G.; Gandini, M.; Barker, A. J.; Ball, J. M.; Srimath Kandada, A. R.; Petrozza, A. Photoinduced Emissive Trap States in Lead Halide Perovskite Semiconductors. *ACS Energy Letters* **2016**, *1* (4), 726−730.
(16) Brenes, R.; Eames, C.; Bulović, V.; Islam, M. S.; Stranks, S. D. The Impact of Atmosphere on the Local Luminescence Properties of Metal Halide Perovskite Grains. *Adv. Mater.* **2018**, *30* (15), 1706208.
(17) deQuilettes, D. W.; Zhang, W.; Burlakov, V. M.; Graham, D. J.; Leijtens, T.; Osherov, A.; Bulović, V.; Snaith, H. J.; Ginger, D. S.; Stranks, S. D. Photo-Induced Halide Redistribution in Organic−Inorganic Perovskite Films. *Nat. Commun.* **2016**, *7*, 11683.
(18) Brivio, F.; Caetano, C.; Walsh, A. Thermodynamic Origin of Photoinstability in the $CH_3NH_3Pb(I_{1-x}Br_x)_3$ Hybrid Halide Perovskite Alloy. *J. Phys. Chem. Lett.* **2016**, *7* (6), 1083−1087.
(19) Anaya, M.; Galisteo-López, J. F.; Calvo, M. E.; Espinós, J. P.; Míguez, H. Origin of Light-Induced Photophysical Effects in Organic Metal Halide Perovskites in the Presence of Oxygen. *J. Phys. Chem. Lett.* **2018**, *9* (14), 3891−3896.
(20) Barker, A. J.; Sadhanala, A.; Deschler, F.; Gandini, M.; Senanayak, S. P.; Pearce, P. M.; Mosconi, E.; Pearson, A. J.; Wu, Y.; Srimath Kandada, A. R.; Leijtens, T.; De Angelis, F.; Dutton, S. E.; Petrozza, A.; Friend, R. H. Defect-Assisted Photoinduced Halide Segregation in Mixed-Halide Perovskite Thin Films. *ACS Energy Letters* **2017**, *2* (6), 1416−1424.
(21) Andaji-Garmaroudi, Z.; Abdi-Jalebi, M.; Guo, D.; Macpherson, S.; Sadhanala, A.; Tennyson, E. M.; Ruggeri, E.; Anaya, M.; Galkowski, K.; Shivanna, R.; Lohmann, K.; Frohna, K.; Mackowski, S.; Savenije, T. J.; Friend, R. H.; Stranks, S. D. A Highly Emissive Surface Layer in Mixed-Halide Multication Perovskites. *Adv. Mater.* **2019**, *31*, 1902374.
(22) McGettrick, J. D.; Hooper, K.; Pockett, A.; Baker, J.; Troughton, J.; Carnie, M.; Watson, T. Sources of Pb(0) Artefacts during XPS Analysis of Lead Halide Perovskites. *Mater. Lett.* **2019**, *251*, 98−101.
(23) Li, Y.; Xu, X.; Wang, C.; Ecker, B.; Yang, J.; Huang, J.; Gao, Y. Light-Induced Degradation of $CH_3NH_3PbI_3$ Hybrid Perovskite Thin Film. *J. Phys. Chem. C* **2017**, *121* (7), 3904−3910.
(24) Zu, F.-S.; Amsalem, P.; Salzmann, I.; Wang, R.-B.; Ralaiarisoa, M.; Kowarik, S.; Duhm, S.; Koch, N. Impact of White Light Illumination on the Electronic and Chemical Structures of Mixed Halide and Single Crystal Perovskites. *Adv. Opt. Mater.* **2017**, *5* (9), 1700139.
(25) Das, C.; Wussler, M.; Hellmann, T.; Mayer, T.; Jaegermann, W. *In Situ* XPS Study of the Surface Chemistry of MAPI Solar Cells under Operating Conditions in Vacuum. *Phys. Chem. Chem. Phys.* **2018**, *20* (25), 17180−17187.
(26) Tsai, H.; Asadpour, R.; Blancon, J.-C.; Stoumpos, C. C.; Durand, O.; Strzalka, J. W.; Chen, B.; Verduzco, R.; Ajayan, P. M.; Tretiak, S.; Even, J.; Alam, M. A.; Kanatzidis, M. G.; Nie, W.; Mohite, A. D. Light-Induced Lattice Expansion Leads to High-Efficiency Perovskite Solar Cells. *Science* **2018**, *360* (6384), 67−70.
(27) Delamarre, A.; Lombez, L.; Guillemoles, J.-F. Contactless Mapping of Saturation Currents of Solar Cells by Photoluminescence. *Appl. Phys. Lett.* **2012**, *100* (13), 131108.
(28) Bercegol, A.; El-Hajje, G.; Ory, D.; Lombez, L. Determination of Transport Properties in Optoelectronic Devices by Time-Resolved Fluorescence Imaging. *J. Appl. Phys.* **2017**, *122* (20), 203102.
(29) Bercegol, A.; Ramos, F. J.; Rebai, A.; Guillemot, T.; Puel, J.-B.; Guillemoles, J.-F.; Ory, D.; Rousset, J.; Lombez, L. Spatial Inhomogeneity Analysis of Cesium-Rich Wrinkles in Triple-Cation Perovskite. *J. Phys. Chem. C* **2018**, *122* (41), 23345−23351.
(30) Katahara, J. K.; Hillhouse, H. W. Quasi-Fermi Level Splitting and Sub-Bandgap Absorptivity from Semiconductor Photoluminescence. *J. Appl. Phys.* **2014**, *116* (17), 173504.
(31) Paul, N.; Guen, V. L.; Ory, D.; Lombez, L. Numerical Model to Extract Materials Properties Map from Spectrally Resolved Luminescence Images. *2017 IEEE 44th Photovoltaic Specialist Conference (PVSC)*, Washington, DC, June 25−30, 2017, pp 70−74.
(32) Braly, I. L.; deQuilettes, D. W.; Pazos-Outón, L. M.; Burke, S.; Ziffer, M. E.; Ginger, D. S.; Hillhouse, H. W. Hybrid Perovskite Films Approaching the Radiative Limit with over 90% Photoluminescence Quantum Efficiency. *Nat. Photonics* **2018**, *12* (6), 355−361.
(33) Cacovich, S.; Matteocci, F.; Abdi-Jalebi, M.; Stranks, S. D.; Di Carlo, A.; Ducati, C.; Divitini, G. Unveiling the Chemical Composition of Halide Perovskite Films Using Multivariate Statistical Analyses. *ACS Appl. Energy Mater.* **2018**, *1* (12), 7174−7181.
(34) Bercegol, A.; Ramos, F. J.; Rebai, A.; Guillemot, T.; Ory, D.; Rousset, J.; Lombez, L. Slow Diffusion and Long Lifetime in Metal Halide Perovskites for Photovoltaics. *J. Phys. Chem. C* **2018**, *122* (43), 24570−24577.
(35) Stranks, S. D.; Burlakov, V. M.; Leijtens, T.; Ball, J. M.; Goriely, A.; Snaith, H. J. Recombination Kinetics in Organic-Inorganic Perovskites: Excitons, Free Charge, and Subgap States. *Phys. Rev. Appl.* **2014**, *2* (3), 034007.
(36) Béchu, S.; Ralaiarisoa, M.; Etcheberry, A.; Schulz, P. Photoemission Spectroscopy Characterization of Halide Perovskites. *Adv. Energy Mater.* **2020**, 1904007.
(37) Lin, H.-J.; Cacovich, S.; Rebai, A.; Rousset, J.; Longeaud, C. Influence of Environment and Light-Stress on the Optoelectronic Properties of Triple-Cation Perovskite Thin Films. *ACS Appl. Mater. Interfaces* **2020**, *12* (17), 19495−19503.
(38) Sun, Q.; Fassl, P.; Vaynzof, Y. Large-Scale Compositional and Electronic Inhomogeneities in $CH_3NH_3PbI_3$ Perovskites and Their Effect on Device Performance. *ACS Appl. Energy Mater.* **2018**, *1* (6), 2410−2416.
(39) Raninga, R. D.; Jagt, R. A.; Béchu, S.; Huq, T. N.; Li, W.; Nikolka, M.; Lin, Y.-H.; Sun, M.; Li, Z.; Li, W.; Bouttemy, M.; Frégnaux, M.; Snaith, H. J.; Schulz, P.; MacManus-Driscoll, J. L.; Hoye, R. L. Z. Strong Performance Enhancement in Lead-Halide Perovskite Solar Cells through Rapid, Atmospheric Deposition of n-Type Buffer Layer Oxides. *Nano Energy* **2020**, *75*, 104946.
(40) Cappel, U. B.; Svanström, S.; Lanzilotto, V.; Johansson, F. O. L.; Aitola, K.; Philippe, B.; Giangrisostomi, E.; Ovsyannikov, R.; Leitner, T.; Föhlisch, A.; Svensson, S.; Mårtensson, N.; Boschloo, G.; Lindblad, A.; Rensmo, H. Partially Reversible Photoinduced Chemical Changes in a Mixed-Ion Perovskite Material for Solar Cells. *ACS Appl. Mater. Interfaces* **2017**, *9* (40), 34970−34978.
(41) Lindblad, R.; Bi, D.; Park, B.; Oscarsson, J.; Gorgoi, M.; Siegbahn, H.; Odelius, M.; Johansson, E. M. J.; Rensmo, H. Electronic Structure of $TiO_2/CH_3NH_3PbI_3$ Perovskite Solar Cell Interfaces. *J. Phys. Chem. Lett.* **2014**, *5* (4), 648−653.
(42) Kerner, R. A.; Schulz, P.; Christians, J. A.; Dunfield, S. P.; Dou, B.; Zhao, L.; Teeter, G.; Berry, J. J.; Rand, B. P. Reactions at Noble Metal Contacts with Methylammonium Lead Triiodide Perovskites: Role of Underpotential Deposition and Electrochemistry. *APL Mater.* **2019**, *7* (4), 041103.
(43) Philippe, B.; Saliba, M.; Correa-Baena, J.-P.; Cappel, U. B.; Turren-Cruz, S.-H.; Grätzel, M.; Hagfeldt, A.; Rensmo, H. Chemical Distribution of Multiple Cation (Rb^+, Cs^+, MA^+, and FA^+) Perovskite Materials by Photoelectron Spectroscopy. *Chem. Mater.* **2017**, *29* (8), 3589−3596.
(44) Veluchamy, P.; Minoura, H. Surface Analysis of Anodic Lead Oxide Films Prepared in Hot Alkaline Solutions. *Appl. Surf. Sci.* **1998**, *126* (3−4), 241−245.
(45) Zu, F.; Amsalem, P.; Ralaiarisoa, M.; Schultz, T.; Schlesinger, R.; Koch, N. Surface State Density Determines the Energy Level Alignment at Hybrid Perovskite/Electron Acceptors Interfaces. *ACS Appl. Mater. Interfaces* **2017**, *9* (47), 41546−41552.
(46) Rondon, S.; Sherwood, P. M. A. Core Level and Valence Band Spectra of PbO by XPS. *Surf. Sci. Spectra* **1998**, *5*, 104.
(47) Jacobsson, T. J.; Correa-Baena, J.-P.; Halvani Anaraki, E.; Philippe, B.; Stranks, S. D.; Bouduban, M. E. F.; Tress, W.; Schenk, K.; Teuscher, J.; Moser, J.-E.; Rensmo, H.; Hagfeldt, A. Unreacted PbI_2 as a Double-Edged Sword for Enhancing the Performance of

https://dx.doi.org/10.1021/acsami.0c06844
ACS Appl. Mater. Interfaces XXXX, XXX, XXX−XXX

Perovskite Solar Cells. *J. Am. Chem. Soc.* **2016**, *138* (32), 10331−10343.
(48) Steirer, K. X.; Schulz, P.; Teeter, G.; Stevanovic, V.; Yang, M.; Zhu, K.; Berry, J. J. Defect Tolerance in Methylammonium Lead Triiodide Perovskite. *ACS Energy Letters* **2016**, *1* (2), 360−366.
(49) Calisi, N.; Caporali, S.; Milanesi, A.; Innocenti, M.; Salvietti, E.; Bardi, U. Composition-Dependent Degradation of Hybrid and Inorganic Lead Perovskites in Ambient Conditions. *Top. Catal.* **2018**, *61* (9−11), 1201−1208.
(50) Christians, J. A.; Schulz, P.; Tinkham, J. S.; Schloemer, T. H.; Harvey, S. P.; Tremolet de Villers, B. J.; Sellinger, A.; Berry, J. J.; Luther, J. M. Tailored Interfaces of Unencapsulated Perovskite Solar Cells for > 1,000 h Operational Stability. *Nature Energy* **2018**, *3* (1), 68−74.
(51) Matteocci, F.; Busby, Y.; Pireaux, J.-J.; Divitini, G.; Cacovich, S.; Ducati, C.; Di Carlo, A. Interface and Composition Analysis on Perovskite Solar Cells. *ACS Appl. Mater. Interfaces* **2015**, *7* (47), 26176−26183.

https://dx.doi.org/10.1021/acsami.0c06844
ACS Appl. Mater. Interfaces XXXX, XXX, XXX−XXX